Supplementary Information to

High-Throughput Approach to Measure Number of Nanoparticles Associated with Cells: Size Dependence and Kinetic Parameters

Ceri J. Richards[a,b], Paula Melero Martinez[a] , Wouter H. Roos[b], and Christoffer Åberg[a*]

[a] Pharmaceutical Analysis, Groningen Research Institute of Pharmacy, University of Groningen, 9713 AV Groningen, Netherlands

[b] Molecular Biophysics, Zernike Institute for Advanced Materials, University of Groningen, 9747 AG Groningen, Netherlands

[*]Email: christoffer.aberg@rug.nl

Particle characterization

Supplementary Table S1. Size and ζ potential characterization of particle dispersions. Particles were either dispersed in phosphate buffered saline (PBS) to assess the pristine particles, or in cell culture medium supplemented with 10% foetal bovine serum (cDMEM) to assess the particles as applied to cells. The dispersions were measured using dynamic light scattering (DLS) and laser Doppler velocimetry to assess particle size and ζ potential, respectively. The values for the pristine particles are in good agreement with those reported by the manufacturer. Moreover, the particles have a low polydispersity index and a negatively charged surface. Upon biomolecular corona formation, the size of the particles dispersed in cDMEM increases and the surface charge shifts towards more neutral values. Furthermore, particles do not appear to agglomerate in cDMEM, in accordance with previous studies on these particles.[1–5] See Supplementary Figure S1 for the corresponding distributions.

Particle	Dispersant	*z* average diameter (nm)[1]	Polydispersity index[1]	Peak diameter (nm)[2]	ζ potential (mV)
40 nm	PBS	49 ± 0.2	0.12 ± 0.005	55 ± 1	−39 ± 4
	cDMEM	80 ± 0.4	0.22 ± 0.02	103 ± 3	−8 ± 0.4
100 nm	PBS	109 ± 0.6	0.02 ± 0.01	113 ± 1	−41 ± 2
	cDMEM	150 ± 1	0.09 ± 0.02	166 ± 2	−8 ± 0.6
200 nm	PBS	207 ± 0.6	0.02 ± 0.008	214 ± 1	−44 ± 3
	cDMEM	255 ± 3	0.06 ± 0.008	276 ± 1	−10 ± 1
500 nm	PBS	535 ± 12	0.04 ± 0.02	561 ± 12	−29 ± 1
	cDMEM	586 ± 24	0.23 ± 0.01	708 ± 27	−8 ± 0.3

[1] From cumulant analysis.
[2] Diameter of main peak from CONTIN analysis.

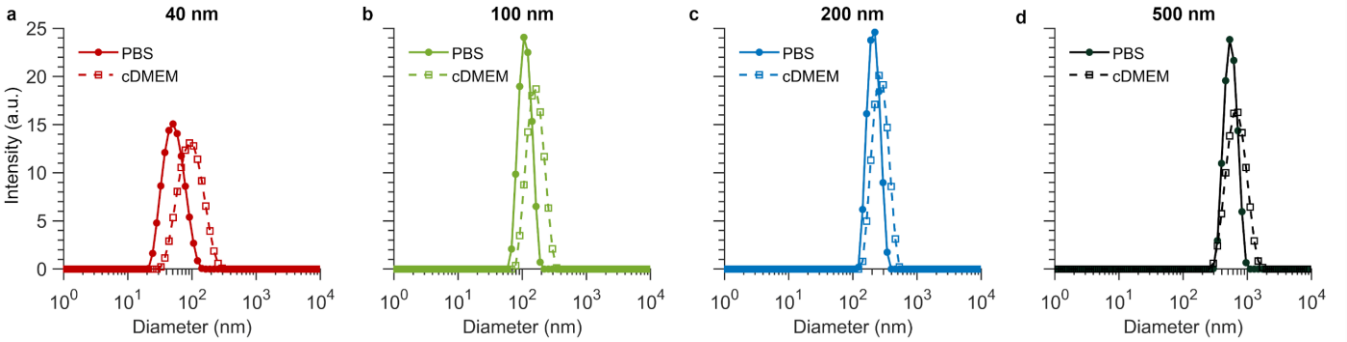

Supplementary Figure S1. Dynamic light scattering (DLS) characterization of nanoparticle size distributions. The nanoparticles were dispersed in either phosphate buffered saline (PBS; filled circles) or cell medium with serum (cDMEM; open squares) to characterize either the pristine particles or particles as exposed to the cells, respectively. (a) 40 nm nanoparticles at a nominal concentration of 2.84×10^{12} particles/ml (100 µg/ml); (b) 100 nm nanoparticles at a nominal concentration of 1.82×10^{11} particles/ml (100 µg/ml); (c) 200 nm nanoparticles at a nominal concentration of 2.28×10^{10} particles/ml (100 µg/ml); and (d) 500 nm nanoparticles at a nominal concentration of 1.46×10^{9} particles/ml (100 µg/ml). A biomolecular corona forms on the particle surface when dispersed in cDMEM, resulting in an increased hydrodynamic diameter compared to pristine particles. This is observed for all particle sizes. We note, however, that as medium is a complex fluid, the size of the shift should not be interpreted in absolute terms. The size distribution mean and peak values are reported in Supplementary Table S1.

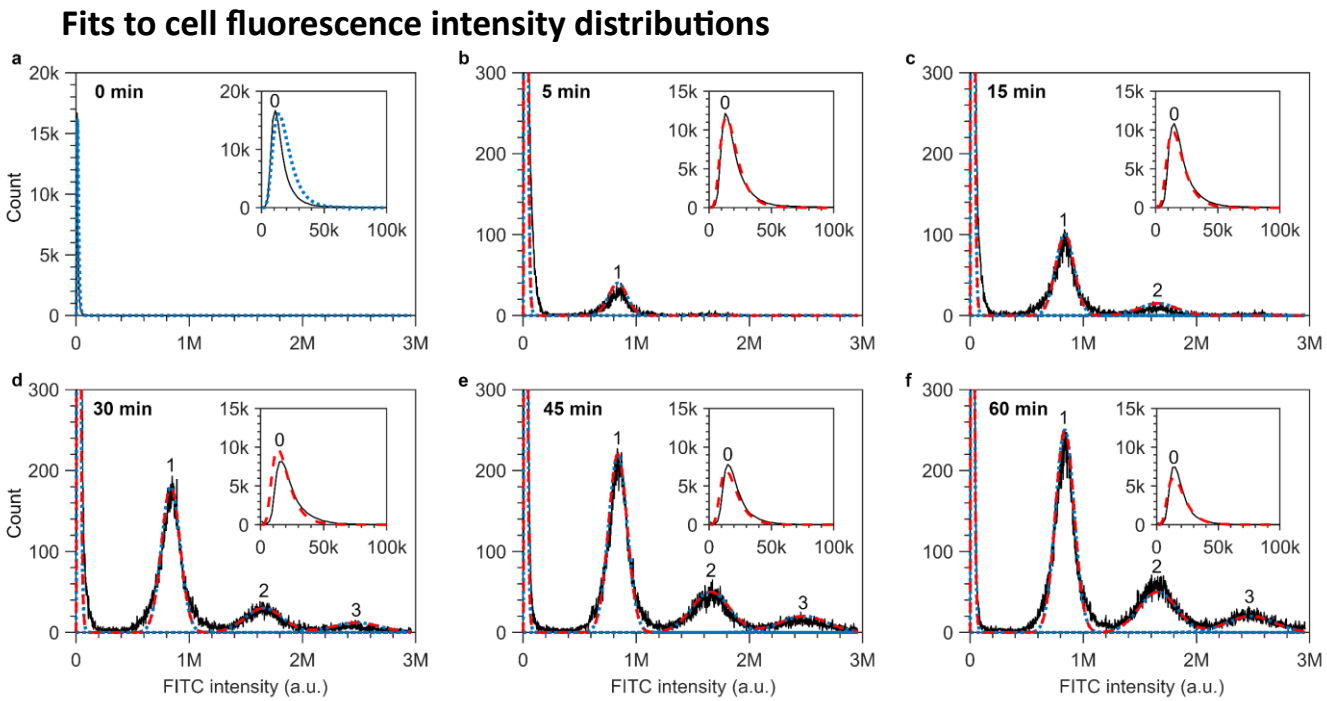

Supplementary Figure S2 Fits to the intensity distributions of HEK cells exposed to 500 nm nanoparticles at low concentration and for short exposure times. Cells were exposed to 500 nm nanoparticles for various timespans at a low nominal particle concentration of 0.58 × 10^9 particles/ml (40 µg/ml) and measured with flow cytometry. The fluorescence intensity in the nanoparticle (FITC) channel was measured for each cell and the distributions of cell intensities are shown (solid black line) for exposure times of (a) 0 min; (b) 5 min; (c) 15 min; (d) 30 min; (e) 45 min; and (f) 60 min. (a) Control cells (not exposed to particles) show a singular peak at approximately 15 000 a.u. This is the background signal of the cells, arising from autofluorescence and the instrument noise level. The peak was fitted with a lognormal distribution (blue dotted line) which approximates the measured intensity distribution well (see inset for a zoomed in view of the control group). (b) Upon exposure to nanoparticles for 5 min, two peaks are observed. The first peak appears at approximately 20 000 a.u. and corresponds to cells with no particles (see inset). The second peak in the cell fluorescence intensity distribution appears at approximately 830 000 a.u. and corresponds to cells with a single associated 500 nm particle. (c) Increasing the particle exposure time, a third peak in the cell fluorescence intensity distribution appears, corresponding to cells with 2 associated nanoparticles. (d) At 30 min particle exposure, a fourth peak occurs corresponding to cells with 3 associated particles. (e–f) At longer particle exposure times, the population of cells within the 0-particle group diminishes, whilst the population within the 1, 2, and 3-particle peaks increases. The results are presented in a linear scale to illustrate the equal spacing between peaks and better appreciate the goodness of fit. Global fitting was performed across all of the data in panels a–f. The 0-particle peak was fitted with a lognormal distribution (blue dotted line), whereas the 1-particle, 2-particle, and 3-particle peaks were fitted with separate gaussian distributions (blue dotted lines). The peak-to-peak distance was constrained to be the same between successive peaks, *i.e.*, the intensity of a single 500 nm particle remains constant irrespective of the number of particles associated with the cell. The total fitted distribution, *i.e.*, the sum of the 0-particle, 1-particle, 2-particle, and 3-

particle peak fits, is shown by the red dashed line. The fitted distributions to each individual peak and the total fitted distribution approximate the data well.

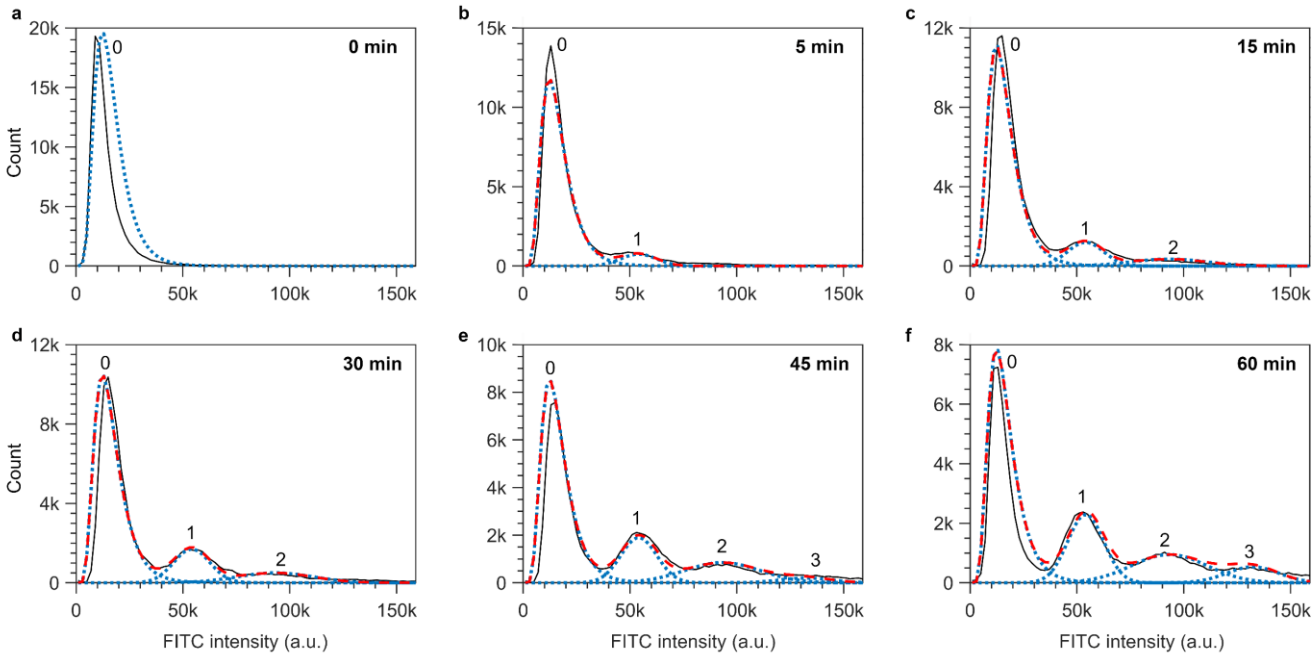

Supplementary Figure S3 Fits to the intensity distributions of HEK cells exposed to 200 nm nanoparticles at low concentration and for short exposure times. Cells were exposed to 200 nm nanoparticles for various timespans at a low nominal particle concentration of 1.71 × 10^9 particles/ml (7.5 µg/ml) and measured with flow cytometry. The fluorescence intensity in the nanoparticle (FITC) channel was measured for each cell and the distributions of cell intensities are shown (solid black line) for exposure times of (a) 0 min; (b) 5 min; (c) 15 min; (d) 30 min; (e) 45 min; and (f) 60 min. (a) Control cells (not exposed to particles) show a singular peak at approximately 15 000 a.u. This is the background signal of the cells, arising from autofluorescence and the instrument noise level. The peak was fitted with a lognormal distribution (blue dotted line) which approximates the measured intensity distribution well. (b) Upon exposure to nanoparticles for 5 min, two peaks are observed. The first peak appears at approximately 20 000 a.u. and corresponds to cells with no particles. The smaller second peak appears at approximately 55 000 a.u. and corresponds to cells with a single associated 200 nm particle. (c) Increasing the particle exposure time, a third peak begins to appear, corresponding to cells with 2 associated nanoparticles. (d) The population of cells in the 1-particle and 2-particle peaks increases upon 30 min particle exposure time. (e) At 45 min particle exposure, a fourth group appears corresponding to cells with 3 associated particles. (f) At 60 min particle exposure, the population of cells within the 0-particle group diminishes, and the 1, 2, and 3-particle peaks become more prominent. The results are presented in a linear scale to illustrate the equal spacing between peaks and better appreciate the goodness of fit. Global fitting was performed across all of the data in panels a–f. The 0-particle peak was fitted with a lognormal distribution (blue dotted line), whereas the 1-particle, 2-particle, and 3-particle peaks were fitted with separate gaussian distributions (blue dotted lines). The peak-to-peak distance was constrained to be the same between successive peaks, *i.e.*, the intensity of a single 200 nm particle remains constant irrespective of the number of particles associated with the cell. The total fitted distribution, *i.e.*, the sum of the 0-particle, 1-particle, 2-particle, and 3-particle peak fits, is shown by the red dashed line. The fitted distributions to each individual peak and the total fitted distribution approximate the data well.

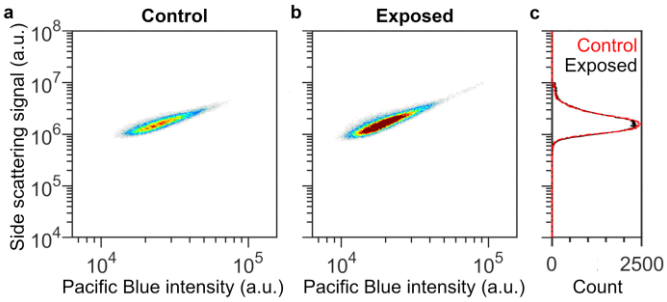

Supplementary Figure S4 Side scattering of HEK cells exposed to 500 nm polystyrene nanoparticles. Cells were exposed to 500 nm nanoparticles for 60 min at a nominal particle concentration of 0.58×10^9 particles/ml (40 µg/ml) and measured with flow cytometry. (a–b) Density plots of side scattering against an empty channel signal (Pacific Blue). The heat map indicates density, where red corresponds to high cell counts and grey to low cell counts. (a) Control cells not exposed to nanoparticles. (b) Cells exposed to particles for 60 min. (c) The distribution of side scattering over cells for the (red) control and (black) particle-exposed cells. The distributions look very similar and separable peaks associated with the signal stemming from 0, 1, 2 *etc.* nanoparticles are not visible, unlike the results for the nanoparticle fluorescence channel (Figure 1). Thus, the scattering signal of these particles is not usable for nanoparticle counting.

Single particle intensity calibration curve

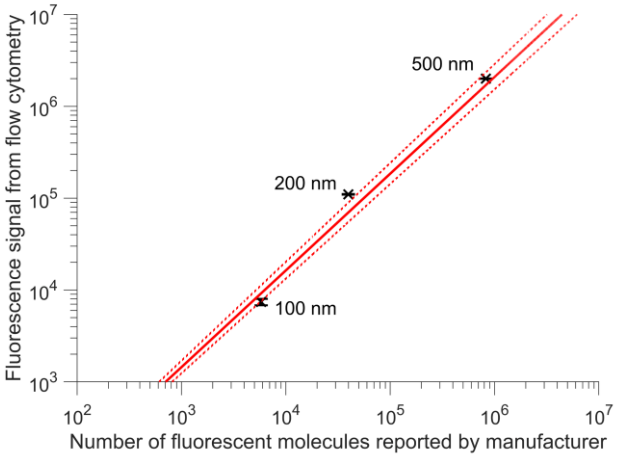

Supplementary Figure S5 Calibration curve for single particle intensities. The intensities of the single particles found using our flow cytometry procedure were plotted as a function of the corresponding number of fluorescent molecules reported by the manufacturer[6] for 500 nm, 200 nm and 100 nm yellow-green nanoparticles (black crosses). Linear fitting was performed on the logarithm of the manufacturer's values as a function of the logarithm of the flow cytometry values maintaining a 0 intercept. This fit yielded the calibration curve (solid red line) and corresponding standard error of the fit (dotted red lines). The expected fluorescence intensity of 40 nm particles measured with flow cytometry was estimated from the calibration curve using the number of fluorescent molecules for the 40 nm particles reported by the manufacturer.[6] This yielded a value of 261 a.u. (231–294 a.u. lower–upper values with standard error).

Shift of cell fluorescence background

We noted a small shift in the background signal upon exposure to 500 nm or 200 nm nanoparticles, *i.e.*, the average intensity of control cells (not exposed to particle dispersion) was slightly lower than the average intensity of the 0-particle population of cells exposed to nanoparticles. This background shift was consistent across different particle exposure times (Supplementary Table S2) and for energy depleted cells (Supplementary Table S3). We suggest that the shift is caused by cellular internalization of small free dye molecules present in the particle dispersion.[7,8] For the smaller particle sizes, the 0-particle group cannot be completely separated from the rest of the cell population so the presence of such a background shift cannot be easily determined. Therefore, to estimate the size of the background shift, cells were exposed to particles at 4 °C to halt particle internalization[5,7] but allow for free dye uptake. The average intensity of cells either exposed or not exposed to particles was then compared. The measured background shift for each particle size is reported in Supplementary Table S4. We note that, though particle internalization is prevented at 4 °C, particles can still bind to the plasma membrane and consequently be measured by flow cytometry. Thus, our values for the background shift are likely to be an overestimate. However, the values we obtained equate to a shift of maximally only 2 nanoparticles (for the 40 nm particles). These values are much smaller than those of interest when determining particle uptake kinetics (Figure 2–4). Therefore, we used these values to perform an adjusted background correction before determining the average number of nanoparticles associated with cells.

Supplementary Table S2 Average fluorescence intensity of cell populations containing no nanoparticles. Average intensities of control cells (not exposed to particles, 0 min) compared to the population of cells containing no particles (0-group) for various timespans (15–60 min) of exposure to 200 nm particles with a nominal concentration of 1.71×10^9 particles/ml (7.5 µg/ml) at 37 °C. The averages are slightly increased compared to control cells and are relatively consistent across the different exposure times, *i.e.*, there is a shift in the background fluorescence of cells with no particles upon exposure to dispersions. The increase is much smaller than the fluorescence intensity determined for a single 200 nm particle. Therefore, we hypothesize that the higher intensity is caused by the cellular internalization of free dye molecules that may be present within the particle dispersion. Values stated are the mean and standard error over three independent experiments.

Exposure time	0 min	15 min	30 min	60 min
200 nm	14 100 ± 90	22 400 ± 230	23 000 ± 390	23 400 ± 600

Supplementary Table S3 Average fluorescence intensity of cell populations at 4 °C. Average intensities of cells maintained at 4°C but not exposed to particles (0 min) compared to cells exposed to particles for various timespans (15–60 min) at 4 °C. The averages are increased compared to control cells and are relatively consistent across the different exposure times. At 4 °C particle internalization does not occur and therefore the increase is attributed to the internalization of free dye and possibly a small fraction of particles that remain bound to cell plasma membranes throughout the sample preparation. Measurements were performed using the same nominal particle concentrations as used for Figure 3, namely 1.14×10^{10} particles/ml (50, 6.26, and 0.40 µg/ml for the 200, 100 and 40 nm particles, respectively). Values stated are mean and standard error over approximately 15 000 cells.

Exposure time	0 min	15 min	30 min	60 min
200 nm	14 900 ± 50	22 500 ± 100	25 000 ± 250	24 100 ± 220
100 nm	14 300 ± 60	19 900 ± 380	24 100 ± 160	28 100 ± 180
40 nm	15 600 ± 40	16 400 ± 80	16 400 ± 80	15 400 ± 70

Supplementary Table S4 Background shift of cells exposed to nanoparticles at 4 °C. Background shift compared to control cells measured using flow cytometry for cells exposed to 200 nm, 100 nm and 40 nm nanoparticles at 4 °C. Measurements were performed using nominal particle concentrations of 1.14×10^{10} particles/ml (50, 6.26, and 0.40 µg/ml for the 200, 100 and 40 nm particles, respectively). Values stated are mean and standard deviation across three exposure times (15, 30, and 60 min).

	200 nm	100 nm	40 nm
Background shift	9 000 ± 1 000	9 700 ± 3 000	530 ± 460
Equivalent number of particles	0.2	1.7	2.2

Fluorescence imaging

It has been reported that nanoparticles are typically trafficked through and accumulate in the endo-lysosomal pathway.[3,9–13] However, due to the limited resolution of fluorescence microscopy, several particles in close proximity to one another, such as those within a lysosome, cannot be separately resolved and will appear as a singular fluorescent object. Therefore, we compared the intensities of the identified fluorescent objects to the intensity of singular nanoparticles adsorbed to glass (Figure 2c). The distribution of intensities of cell-associated fluorescent objects mostly overlaps with the intensity distribution of singular particles, but a small population of multi-particle objects is also present (elongated tail in Figure 2c). The average intensity of particles on glass was 70 631 a.u. after correcting for the intensity of the image background. Fluorescent objects with an intensity of less than 105 947 a.u. (1.5× the average single particle intensity) were classified as single particles within cells, objects with an intensity of 105 947–176 579 a.u. (1.5–2.5× the average single particle intensity) were classified as two particles, *etc*. As such, fluorescent objects which comprised of 1–3 particles were identified. Based on this, the number of particles for each cell was corrected yielding an average number of particles per cell of 20 ± 2. Without the correction this value was 18 ± 2, which still corresponds well to the flow cytometry results (Figure 2d).

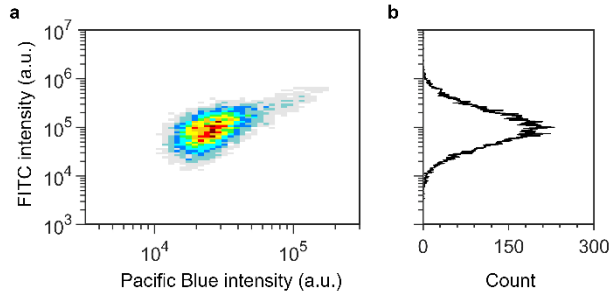

Supplementary Figure S6 Association of 100 nm nanoparticles to cells after 2 h exposure measured using flow cytometry. Cells were exposed to 100 nm nanoparticles for 2 h at a nominal concentration of 1.14×10^{10} particles/ml (6.26 µg/ml) and then measured by flow cytometry. (a) Density plot of the particle signal (FITC) against an empty channel signal (Pacific Blue) from a representative replicate from one of the independent experiments presented in Figure 2d. The heat map indicates density, where red corresponds to high cell counts and grey to low cell counts. (b) Histogram of the particle (FITC) signal per cell. The data show a broad distribution where singular particle peaks can no longer be observed.

Estimate of extracellular particle numbers

Being able to quantify the number of particles associated with cells has the added advantage that we are also able to estimate the loss of particles in the extracellular medium due to uptake. We exemplify the approach based on Figure 3. The results in that figure are from cells that were exposed to a 0.5 ml particle dispersion at a nominal concentration of 1.14×10^{10} particles/ml (50, 6.26, and 0.40 µg/ml for the 200, 100 nm, and 40 nm particles, respectively), meaning that the total number of particles in the volume was ~5.70×10^{9}. 200 000 cells were seeded which each took up ~200 particles after 5 h on the average (Figure 3), meaning a total of ~4×10^{7} particles. This is a very small fraction (~0.7%) of the original number of particles, showing that the number of particles is in excess compared to the uptake.

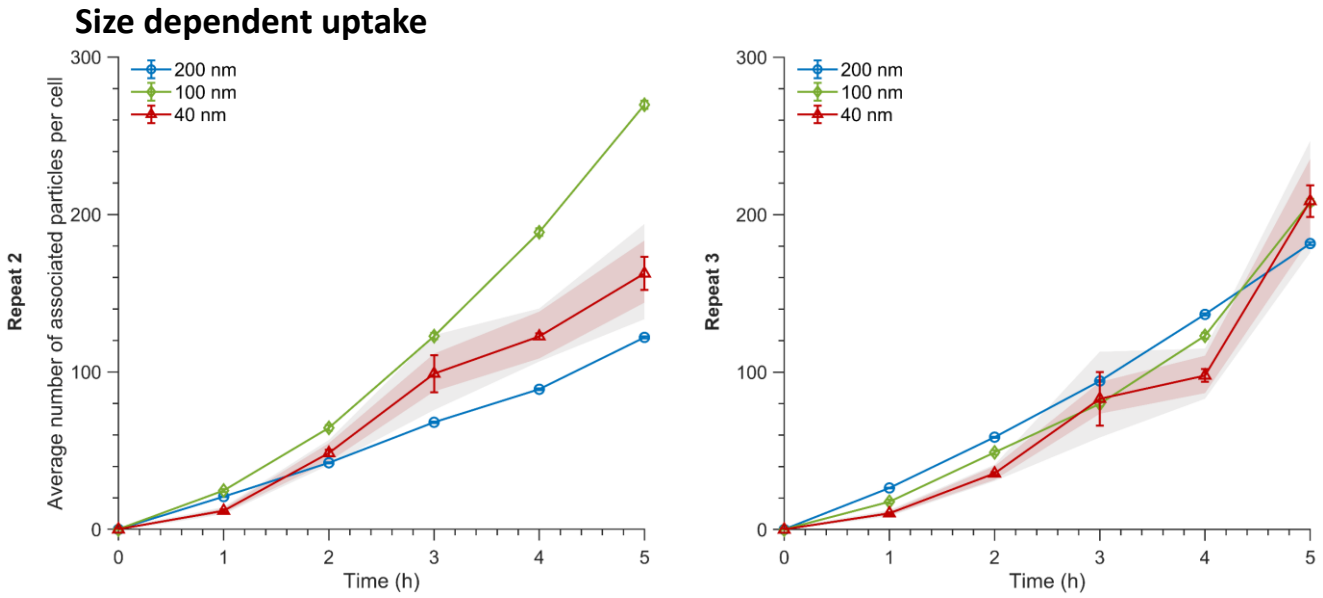

Supplementary Figure S7 Association kinetics of 40, 100 and 200 nm particles (repeat experiments of Figure 3). Association kinetics of particles exposed to cells for various timespans for the 200 nm particles, 100 nm particles and 40 nm particles at a nominal concentration of 1.14×10^{10} particles/ml (50, 6.26, and 0.40 µg/ml, respectively) for all particle sizes for two independent experiments (another independent experiment is reported in Figure 3). The average fluorescence intensity of ~30 000 cells was measured by flow cytometry and converted to the average number of particles associated with cells. A correction was applied due to the discrepancies between the nominal concentrations and the actual measured particle concentrations (see Materials and Methods for details). Mean values are the average over cells from each independent experiment and the error is given by the standard error of the mean. The pink shading shows the mean values calculated using the lower and upper estimates of the fluorescence intensity of a single 40 nm particle (Supplementary Figure S5; for details see the 'Materials and Methods' section). The grey shading shows the standard error of the mean when using the upper and lower estimates.

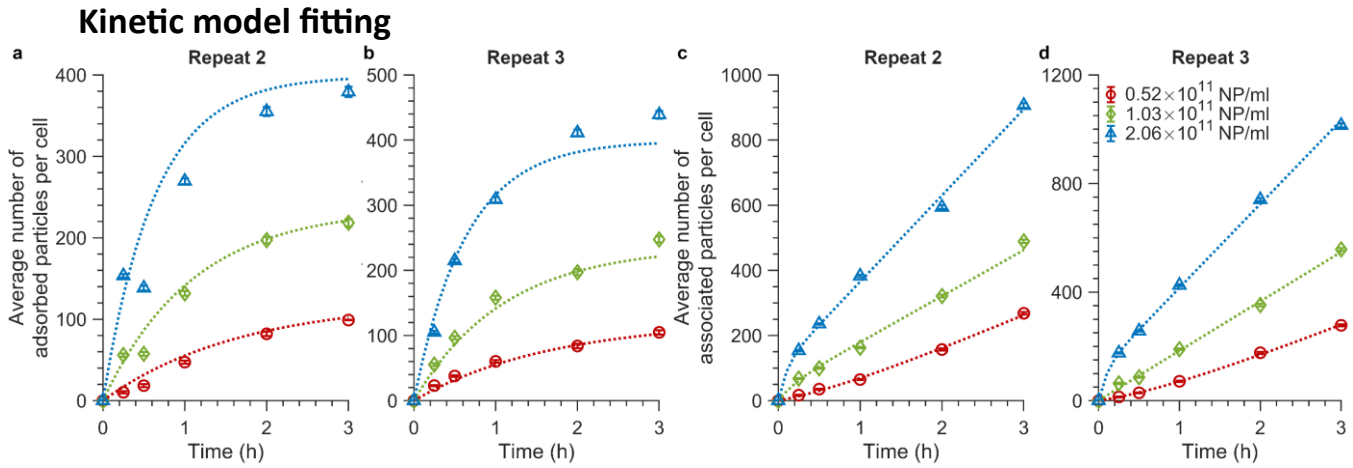

Supplementary Figure S8 Adsorption and association kinetics of 100 nm nanoparticles at different concentrations (repeat experiments of Figure 4). Association kinetics of 100 nm particles exposed to cells for various timespans for two independent experiments (another independent experiment is reported in Figure 4). The average fluorescence intensity of ~15 000 cells was measured by flow cytometry and converted to average number of particles associated with cells. Three particle concentrations were investigated: 0.52×10^{11}, 1.03×10^{11}, and 2.06×10^{11} particles/ml (or 28.6, 56.6, and 113.2 µg/ml). The concentration values are corrected from the nominal concentrations based on the number of particles measured in a known volume using fluorescence microscopy (see 'Materials and Methods' for details; the corresponding nominal concentrations are 0.455×10^{11}, 0.909×10^{11}, and 1.82×10^{11} particles/ml or 25, 50, and 100 µg/ml). The error is given by the standard error of the sample. (a,b) Adsorption kinetics of particles exposed to cells at 4 °C, for which only adsorption and desorption processes are present, for the two independent experiments. Equation (4) was fitted (dotted lines) to the experimental data (symbols) to good agreement. (c,d) Total association kinetics (adsorbed and internalized particles) of the 100 nm particles exposed to cells at 37 °C, for which adsorption, desorption and internalization occur, for the two independent experiments. Equation (3) (in rewritten form) was fitted across the various particle concentrations with k_i as a global (shared) parameter (see 'Materials and Methods' section for details). The fits (dotted lines) describe the experimental data (symbols) well.

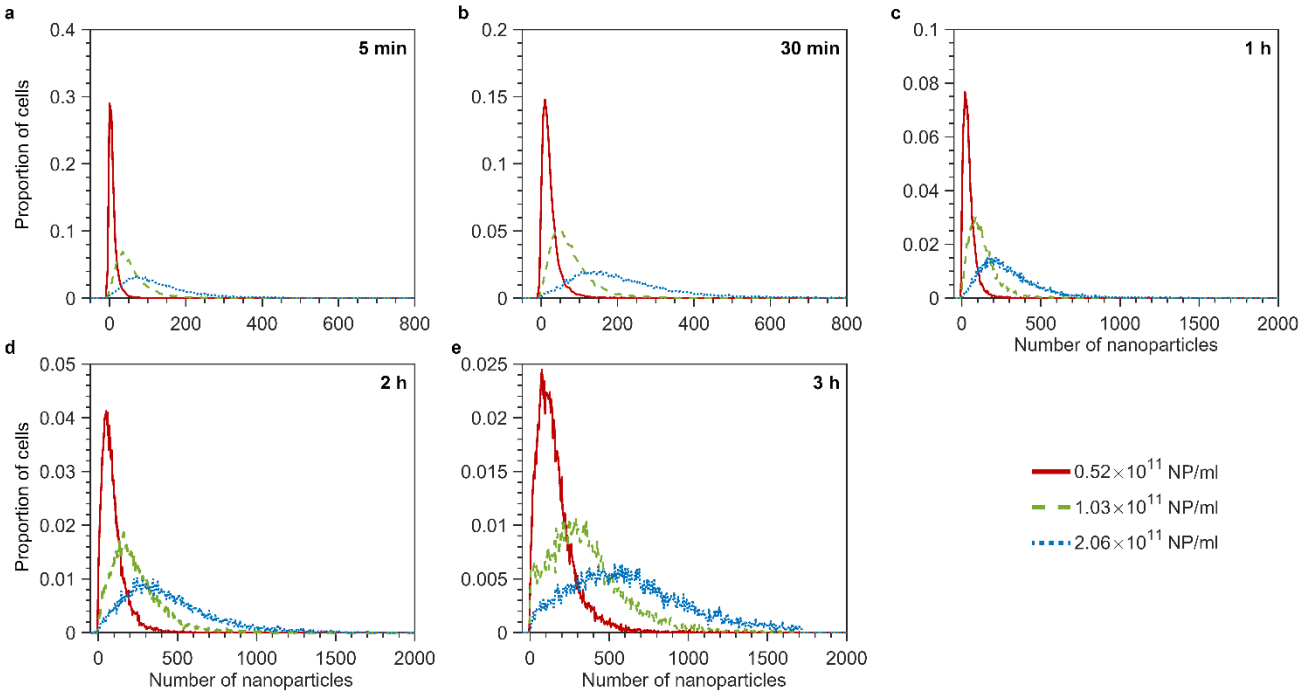

Supplementary Figure S9 Distributions of the number of nanoparticles per cell for the data presented in Figure 4c. 100 nm particles were exposed to cells for various timespans. The fluorescence intensity of ~15 000 cells was measured by flow cytometry and converted to the number of particles associated with each cell using the procedure outlined in the main text. The distributions were then formed using a bin size of 5 nanoparticles. Three particle concentrations were investigated: 0.52 × 10^{11}, 1.03 × 10^{11}, and 2.06 × 10^{11} particles/ml (or 28.6, 56.6, and 113.2 µg/ml). The concentration values are corrected from the nominal concentrations based on the number of particles measured in a known volume using fluorescence microscopy (see 'Materials and Methods' for details). The corresponding nominal concentrations are 0.455 × 10^{11}, 0.909 × 10^{11}, and 1.82 × 10^{11} particles/ml (or 25, 50, and 100 µg/ml), respectively. The data shown are from one independent experiment corresponding to the data presented in Figure 4c. Cells exposed to particles for (a) 15 min, (b) 30 min, (c) 1 h, (d) 2h, and (e) 3 h. With increasing exposure time, the distributions skew to higher numbers of nanoparticles and also become broader. This likewise occurs for increasing particle concentrations. For all exposure conditions some cells still had no associated nanoparticles, whereas the highest number of nanoparticles any cell in the population had increased with concentration and exposure time. The results are presented in a linear scale to more clearly illustrate the large cell-to-cell variability.

Particle concentration measurements

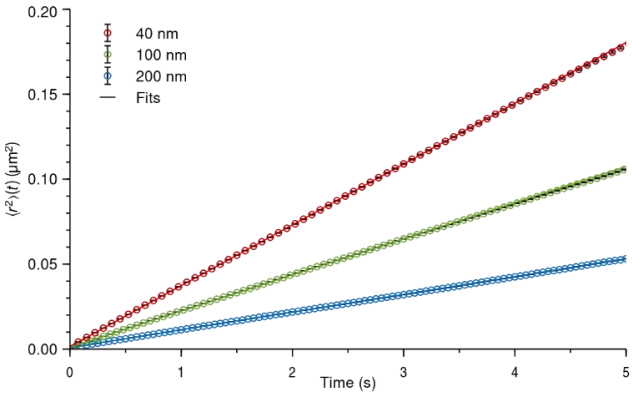

Supplementary Figure S10 Mean square displacement of 40, 100, and 200 nm particles dispersed in glycerol. 40, 100, and 200 nm particles were dispersed in glycerol at a nominal concentration of 1.14×10^9 particles/ml (0.04, 0.63, and 5 µg/ml, respectively) and imaged using fluorescence microscopy. The number of fluorescent objects within the imaged volumes were counted to calculate the actual particle concentrations (see Material and Methods section 'Nanoparticle dispersion characterisation' of the main text). To validate whether the counted particles were singular or agglomerates, timelapse fluorescence imaging of the particles dispersed in glycerol was performed separately. The ImageJ/Fiji[14,15] plugin TrackMate[16] was used to track the fluorescent objects and their mean square displacement (time and ensemble averaged) was calculated from the particle trajectories. The figure shows experimental data together with corresponding linear fits. We included an intercept in the fitting function to account for localisation imprecision, and for the same reason excluded the very first datapoint at time equal to 0 s. The diffusion coefficients of the tracked objects were calculated from the slopes of the linear fits. From the diffusion coefficient the average object diameter was calculated from the Stokes-Einstein equation using the viscosity of 100% glycerol at 25 °C.[17] The calculated object diameters were 53.3 ± 0.1 nm, 89.6 ± 0.1 nm and 182.4 ± 0.1 nm for the 40 nm, 100 nm and 200 nm diameter particles, respectively (error given by standard error of the fit). Therefore, the particles do not tend to agglomerate in glycerol and the counted number of objects is indicative of the actual number of particles within the imaging volumes.

References

1 A. Lesniak, A. Salvati, M. J. Santos-Martinez, M. W. Radomski, K. A. Dawson and C. Åberg, *Journal of the American Chemical Society*, 2013, **135**, 1438–1444.

2 J. A. Varela, M. G. Bexiga, C. Åberg, J. C. Simpson and K. A. Dawson, *Journal of Nanobiotechnology*, 2012, **10**, 39.

3 N. Vtyurina, C. Åberg and A. Salvati, *Nanoscale*, 2021, **13**, 10436–10446.

4 C. J. Richards, M. Ahmadi, M. C. A. Stuart, B. J. Kooi, C. Åberg and W. H. Roos, *Nanoscale*, 2023, **15**, 248–258.

5 C. J. Richards, T. C. Q. Burgers, R. Vlijm, W. H. Roos and C. Åberg, *ACS Nano*, 2023, **17**, 16517–16529.

6 FluoSpheres® Fluorescent Microspheres, www.probes.com, (accessed January 2023)

7 A. Salvati, C. Åberg, T. dos Santos, J. Varela, P. Pinto, I. Lynch and K. A. Dawson, *Nanomedicine: Nanotechnology, Biology and Medicine*, 2011, **7**, 818–826.

8 T. Tenuta, M. P. Monopoli, J. Kim, A. Salvati, K. A. Dawson, P. Sandin and I. Lynch, *PLOS ONE*, 2011, **6**, e25556.

9 T.-G. Iversen, T. Skotland and K. Sandvig, *Nano Today*, 2011, **6**, 176–185.

10 P. Sandin, L. W. Fitzpatrick, J. C. Simpson and K. A. Dawson, *ACS Nano*, 2012, **6**, 1513–1521.

11 D. Vercauteren, H. Deschout, K. Remaut, J. F. J. Engbersen, A. T. Jones, J. Demeester, S. C. De Smedt and K. Braeckmans, *ACS Nano*, 2011, **5**, 7874–7884.

12 L. Yang, L. Shang and G. U. Nienhaus, *Nanoscale*, 2013, **5**, 1537–1543.

13 J. Reinholz, C. Diesler, S. Schöttler, M. Kokkinopoulou, S. Ritz, K. Landfester and V. Mailänder, *Acta Biomaterialia*, 2018, **71**, 432–443.

14 C. A. Schneider, W. S. Rasband and K. W. Eliceiri, *Nature Methods*, 2012, **9**, 671–675.

15 J. Schindelin, I. Arganda-Carreras, E. Frise, V. Kaynig, M. Longair, T. Pietzsch, S. Preibisch, C. Rueden, S. Saalfeld, B. Schmid, J.-Y. Tinevez, D. J. White, V. Hartenstein, K. Eliceiri, P. Tomancak and A. Cardona, *Nature Methods*, 2012, **9**, 676–682.

16 J.-Y. Tinevez, N. Perry, J. Schindelin, G. M. Hoopes, G. D. Reynolds, E. Laplantine, S. Y. Bednarek, S. L. Shorte and K. W. Eliceiri, *Methods*, 2017, **115**, 80–90.

17 J. B. Segur and H. E. Oberstar, *Industrial & Engineering Chemistry*, 1951, **43**, 2117–2120.